An updated model of Rietveld structure refinement of Na/K-feldspar

Shanke Liu*, Jiaju Li, Jianming Liu

Key Laboratory of Mineral Resources, Institute of Geology and Geophysics, Chinese Academy of Sciences, No. 19, Beitucheng Western Road, Chaoyang District, Beijing, 100029, People's Republic of China

ABSTRACT

Alkali feldspar is highly abundant on earth, and studies of its structure are very important in geology. When a single crystal is unavailable for alkali feldspar in some cases, X-ray powder diffraction (XRPD) is essential. However, some problems on extracting high-quality structural data of Na/K–feldspar from XRPD exist, such as deviation of Al/Si–O bond length from expected value, difficulty in identifying Al and Si elements with similar scattering power because of their same crystallographic site, and severe overlapping of diffraction peaks caused by a low symmetry of crystal structure. To extract high-quality structural data, two equations related to Si/Al–O bond length and Si/Al occupancy in terms of the crystal structure database were respectively calculated for albite and microcline. A better model was established by tactically combining the two equations and soft distance constraints for Al/Si–O bond lengths. Application of the updated model successfully obtained high-quality structural data from two different samples using Bragg–Brentano XRPD via the Rietveld method with the general structure analysis system. The reliability of these structural data for low-symmetry albite and microcline was discussed by comparing the data with the results of previous studies.

Keywords: alkali feldspar; crystal structure; Rietveld refinement; X-ray powder diffraction.

INTRODUCTION

Feldspars are tectosilicates with every oxygen atom shared by adjacent silicon or aluminum tetrahedron. The tetrahedrons are arranged in four-member rings that are stacked to form "crankshafts" parallel to the a–axis of the monoclinic or triclinic structure (Figure 1). Four tetrahedrons are named by a pair of t_1 structures and a pair of t_2 structures for monoclinic structure and by a pair of t_1o and t_1m structures and a pair of t_2o and t_2m structures for triclinic structure (Figure S1). The crankshafts are joined together in an open structure with large voids to hold the alkalis or calcium (Figure 1). Sanidine, orthoclase, and microcline are all polymorphs of potassium-rich alkali feldspar ($KAlSi_3O_8$). The structures of these three minerals principally differ in the ordering

of aluminum and silicon among the four tetrahedrons in each tetrahedral ring. High sanidine is fully disordered with a statistically random Al–Si distribution; on average, each tetrahedron has 0.25 Al atoms and 0.75 Si atoms. If a sanidine crystal is cooled slowly from high temperature, Al–Si ordering will occur with the Al atoms preferring one of the two pairs of tetrahedrons in each ring. Low sanidine and orthoclase are successively more ordered versions of the high sanidine structure. For these monoclinic minerals, the center of symmetry in each ring must be preserved, and this requires a random distribution of Al and Si on each distinct tetrahedral site (t_1 or t_2). For example, 80% of the Al might be in t_1 tetrahedron and 20% of the Al in t_2 tetrahedron. To maintain the center of symmetry, 80% of the Al must be distributed randomly
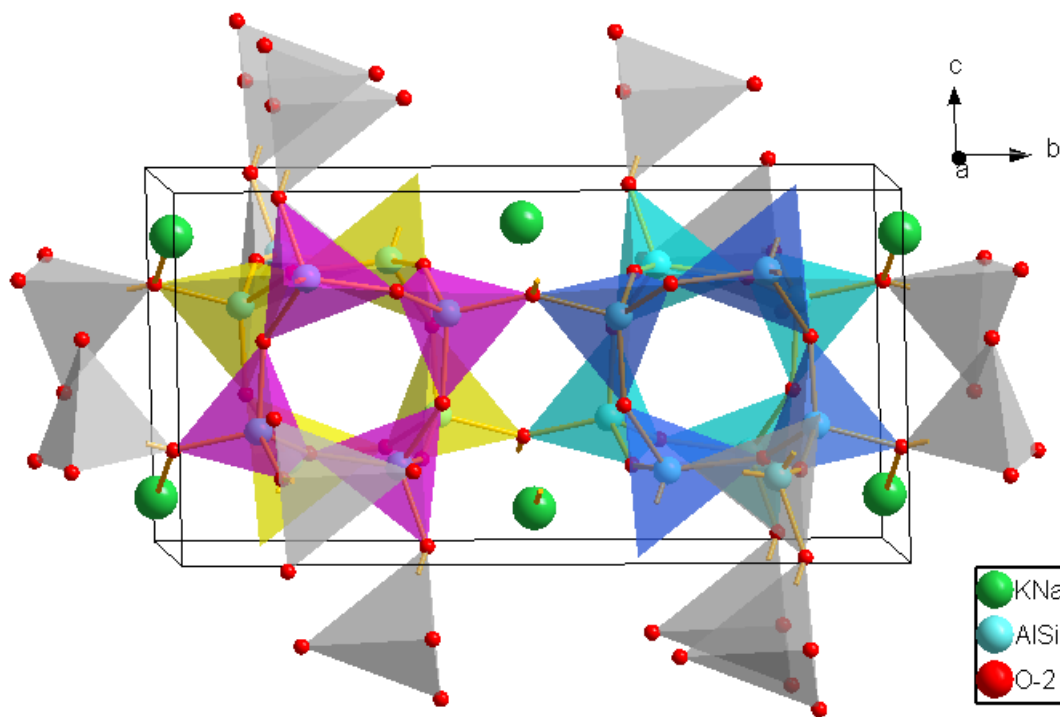
Figure 1. K/Na–feldspar structure in a perspective view along the a axis (four rings were shown in the unit cell with pink, blue, green and yellow, respectively, and others in gray).

among all of the t_1 tetrahedron and 20% of the Al must be distributed randomly among all the t_2 tetrahedrons. At lower temperatures, the ordering between t_1 and t_2 will be complete, and ordering of the Al on the two (formerly) equivalent t_1 tetrahedrons will begin. This ordering will destroy the center of symmetry, and the mineral will become triclinic microcline. Maximum microcline would be a fully ordered mineral with all of the Al on one of the two sites, i.e., t_1o or t_1m. The structure of Na–feldspar ($NaAlSi_3O_8$) is similar to that of K–feldspar ($KAlSi_3O_8$). However, albite is triclinic due to the smaller ionic radii of Na.

Numerous crystal structure determinations of minerals mainly rely on single-crystal X-ray diffraction (SC–XRD), and the structure determination of minerals exhibits several typical difficulties. The chemical composition is often variable, requiring a distinct contrast in scattering power of the different elements to allow for successful identification. Two (or more) chemical elements can occupy the same crystallographic site, which makes it difficult for X-ray diffraction to identify different elements with similar scattering power. This finding is true for alkali feldspar, which is abundant on earth. When Al and Si distributions in feldspar were calculated by X-ray intensities, only the highest quality data that were thoroughly corrected for absorption and extinction would yield meaningful results (Ribbe, 1983). The reason is the

similar scattering powers of Al and Si as well as the high correlation among scale factors, thermal parameters, and extinction correction parameters (Ribbe, 1983). Therefore, the determination of Al/Si distribution in alkali feldspar using X-ray was achieved by indirect methods. All kinds of models for determining Al/Si distribution via X-ray method have been reviewed and presented by several authors (Ribbe, 1983; Kroll and Ribbe, 1987; Tribaudino et al., 2010, 2011). Methods for determining the Al/Si distribution in alkali feldspars among nonequivalent tetrahedral sites are all model dependent, and different types of feldspars have been introduced into those models. An internal consistency possibly exists among those models, with $\sum t1=2t_1$ or (t_1o+t_1m) (t_1, t_1o, and t_1m refer to the Al content in t_1, t_1o, and t_1m tetrahedron, respectively) estimated to be about ±0.02 and $\Delta t_1=(t_1o–t_1m)$ to be about ±0.03 (Kroll and Ribbe, 1987).

When a single crystal is unavailable for alkali feldspar, X-ray powder diffraction (XRPD) may be the best choice to extract the structural data. In addition, Bragg–Brentano XRPD (BB–XRPD) with Cu $K\alpha$ radiation may be the most extensively used instrument in the laboratory and has a major advantage in terms of cost and convenience. Basing on comparison data between BB–XRPD and SC–XRD, Zucchini et al. (2012) concluded that the two methods complement each other. Therefore, the structural refinement from BB–XRPD will be still worthy of

exploration. However, few papers reported the structure of natural alkali feldspar extracted from BB–XRPD. First, the main reason is that the single crystal of feldspar can be obtained even though most feldspars display extensive cross-hatched twinning. This twinning makes single-crystal diffraction difficult for obtaining accurate structure data. Second, the low symmetry (triclinic or monoclinic) of the feldspar structure results in some overlapped diffraction peaks. These peaks confer difficulty in extracting high-quality structural data from BB–XRPD, in particular if low resolution experimental setting is used such as in BB–XRPD with Cu target. Third, the authors found that powder refinements provide very close average Al/Si–O distances to those from SC–XRD, but the spread of distances was very wide for albite and microcline in this paper, similar to what Smrcok (1995) found for kaolinite. Although an introduction of soft distance constraints (SDCs) for Al/Si–O bond lengths efficiently improved the accuracy and precision of the structural data for kaolinite (Smrcok, 1995), this method failed to obtain expected values by applying SDCs for Al/Si–O bond lengths in albite and microcline structures because their structures are different from those of kaolinite. In addition, Al and Si elements occupy the same crystallographic site in feldspar, which often makes it very difficult for X-ray diffraction to identify them because of similar scattering power. All structures of microcline and albite in the ICSD database (version 2009–1) and the American Mineralogist Crystal Structure Database are solved and refined by SC–XRD, which supports aforementioned reasons.

A preliminary study on the Rietveld refinement of microcline had been discussed in the paper of Liu (2015). In this study, the authors extended the refinement to albite, and two samples, albite and perthite, were refined by an updated model. The reliability of structural parameters was evaluated in terms of published values mainly obtained from SC–XRD.

SAMPLES AND METHODS
Samples

An sample including 99.3% albite and 0.7% quartz was mined from Jiaodong peninsula, Shandong Province, China (denoted as ALBITE), and a perthite sample (69.9% albite, 28.5% microcline, and 1.6% quartz) was obtained from Bayan Obo, Inner Mongolia, China (denoted as PERTHITE). Both two samples contained minor quartz, but they were not purified because the existence of minor quartz had slight effect on the structure refinement of alkali feldspar, and one of the objectives of this study was to explore the potential of the Rietveld method. Both two samples were pulverized and ground in an agate mortar and pestle with ethanol as auxiliary agent.

Measurement of XRPD pattern

Step-scanned patterns were measured using a Rigaku D/max–2400 Bragg–Brentano diffractometer fitted with a graphite diffracted–beam monochromator (Rigaku Corporation, Japan). The sample was prepared by the backloading method to reduce the effects of preferred orientation. The details of measurement are shown in Table 1.

Rietveld refinement by GSAS

The Rietveld method, initially proposed by Rietveld (1967, 1969), has significantly improved over the last 40 years. This method has become an effective tool for reliable structural analysis of various compounds with a three-dimensional order.

The computer program package GSAS (Larson and Von Dreele, 2004) and its graphical interface EXPGUI (Toby, 2001), which are freely available, were used for structural refinements. The quality of fit for the experimental and calculated profiles obtained by the programs was tested using LaB_6 standard (SRM 660b, National Institute of Standards and Technology, USA) XRPD pattern. The

Table 1. XRPD pattern measurement conditions.

Instrument	Rigaku Dmax2400
Radiation	Cu–anode tube; operated at 40 kV and 60 mA
Wavelength	Cu $K\alpha$ = 1.5418 Å; Cu $K\alpha_1$ = 1.54060 Å; Cu $K\alpha_2$ = 1.54439 Å
Optics	Bragg–Brentano; Divergence slit = 1°; Scatter slit = 1°; Receiving slit = 0.15 mm
Specimen Holder	Rectangular aluminium plates with a rectangular window
Detection	Graphite diffracted beam monochromator set for Cu $K\alpha$;
	NaI scintillator detector
Acquisition	Angular range in 2θ = 12°–122° for albite and in 2θ = 10°–140° for perthite; Step size = 0.02°; Counting time =1s step^{-1}

PM

instrumental parameter file was obtained from the XRPD pattern of LaB_6 standard.

The starting atomic coordinates, cell parameters, equivalent isotropic displacement parameters, and space groups of microcline, albite, and quartz were based on Dal Negro et al. (1978), Ribbe et al. (1969), and d'Amour et al. (1979), respectively. The background was modeled with eight-term shifted Chebyschev polynomial function. The peak-profile parameters were modelled using a modified TCH-pseudo-Voigt function modified by axial divergence (Finger et al., 1994) and as implemented in Profile function 3 in GSAS. Preferred orientation was described using the spherical harmonics function. Microstrain anisotropy was modeled using an empirical extension, and variables L11 to L23 were refined (Larson and Von Dreele, 2004). However, apart from the major phase, the samples ALBITE and PERTHITE contained 0.7% and 1.6% quartz, respectively, based on quantitative phase analysis. The impurity phase has a negligible amount and thus only slightly affects the overall refinement. Accordingly, only its individual cell and phase fraction parameters were optimized during refinement. The profile parameters of the minor quartz phase were approximated by constraining them to be the same as those of the major phase in ALBITE and PERTHITE, respectively.

Presentation of an updated refining model and two linear relations

In published papers, Al/Si occupancies were calculated from Al/Si–O bond lengths or other lattice parameters obtained from SC-XRD or XRPD (Ribbe, 1983; Kroll and Ribbe, 1987). A general idea on the model presented in this paper had been reported in Liu's paper (2015). In this paper, Al/Si site occupancies were also calculated by the lattice parameter method of Kroll and Ribbe (Kroll and Ribbe, 1987), and $t_2o=t_2m$ (t_2o and t_2m refer to the Al content in t_2o and t_2m tetrahedrons, respectively) was assumed. The Al occupancies in t_1o, t_1m, t_2o, and t_2m tetrahedrons were modified before refining atomic coordinates. When these atomic coordinates were refined, the constraint of Al/Si–O bond lengths (SDC) based on their corresponding Al/Si occupancies were applied to avoid a large deviation during refinement. The calculated Al occupancies and the constrained Al/Si–O bond lengths were manually updated until the refinement reached convergence. To accomplish the application of SDCs, the authors presented two linear regression equations (Figure S2) of the mean T–O bond length ($<T–O>$) versus corresponding Al/(Al+Si) ratio in a tetrahedron using published structural data in ICSD database, version 2009–1 of albite (the authors considered 25 sets of data: 23 from SC–XRD data, 1 from XRPD data, and 1 from neutron diffraction data) (Ferguson et al., 1958; Ribbe et al., 1962; Phillips et al., 1971; Prewitt et al., 1976; Keefer

and Brown, 1978; Winter et al., 1979; Harlow and Brown Jr., 1980; Wenk and Kroll, 1984; Phillips et al., 1989; Armbruster et al., 1990; Downs et al., 1994; Finger et al., 1994; Meneghinello et al., 1999) and microcline (overall 18 sets of data from SC–XRD) (Bailey and Taylor, 1955; Brown, 1961; Brown and Bailey, 1964; Finney and Bailey, 1964; Dal Negro et al., 1978; Ribbe ,1979; Blasi et al., 1981, 1984, 1987; Allan and Angel, 1997). From Figure S2, the relationship between T–O bond length vs. Al site occupancy (t_i) was as follows:

albite:

$<T–O>/(Å)=1.6109(6)+0.1321(16)t_i$ ($0≤t_i≤1$, $1.6109≤<T–O>≤1.7430$)   (1)

microcline:

$<T–O>/(Å)=1.6109(5)+0.1333(12)t_i$ ($0≤t_i≤1$, $1.6109≤<T–O>≤1.7442$)   (2)

The linear correlation coefficient R^2 is equal to 0.9851 for albite and 0.9935 for microcline, respectively, and a good linear relationship exists between T–O bond length vs. Al site occupancy. Equations (1) and (2) show that the mean T–O bond length in each tetrahedron ($<T–O>$) of albite is very close to that of microcline. The constrained distance between Al/Si and O atoms in t_1o, t_1m, t_2o, and t_2m tetrahedrons was calculated from Equation (1) for albite and Equation (2) for microcline. The average of the four independent T–O distances was taken in every tetrahedron. An uncertainty of ±0.01 Å and a restraint weight of 50 were applied [the distance weight is the product of the weight factor and $1/esd(distance)^2$]. To show the effectiveness of this refinement strategy, the authors applied two different models for refining albite in the ALBITE sample as a test: one model did not apply SDCs (the refinement strategy was denoted as Albite–N) and another model applied SDCs (the refinement strategy was denoted as Albite). Except whether SDCs were applied or not, other strategies were all the same in both models. Results from two different models showed that these structural data of albite from the second model were closer to published data. An updated refining model (Figure 2) was established to extract high-quality structural data from BB–XRPD. Angel et al. (2013) showed that the average $<T–O>$ lengths were relatively insensitive to chemical composition. Wang et al. (1998) proved that the observed composition approached to a theoretical formula for albite from ALBITE. Therefore, theoretical chemical formulas of microcline ($KAlSi_3O_8$) and albite ($NaAlSi_3O_8$) were assumed in the structural model. The structural parameters in the last cycles were presented upon reaching convergence. Relevant .cif files were submitted and are available at the Journal site.

RESULTS

To decrease the uncertainty introduced by different degrees of Al/Si order and very close chemical

PM
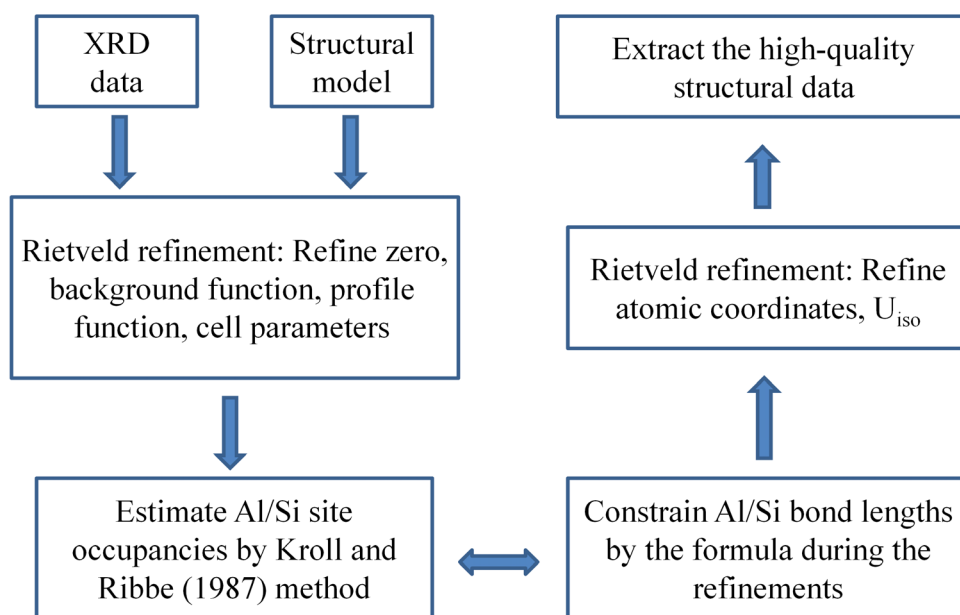
Figure 2. An updated model for extracting the high-quality structural data from BB–XRPD using Rietveld refinement.

compositions, reference values of albite and microcline were obtained from an average of eight groups of albite structural data from six different localities (Ribbe et al., 1962; Ribbe et al., 1969; Harlow and Brown Jr, 1980; Armbruster et al., 1990; Downs et al., 1994; Meneghinello et al., 1999) and an average of seven groups of microcline structural data from six different localities (Brown, 1961; Brown and Bailey, 1964; Dal Negro et al., 1978; Blasi et al., 1984; Blasi et al., 1987; Allan and Angel, 1997). The structural data in this paper were compared to those averages obtained from the reference data. The authors defined a few terms and used these terms throughout the remainder of the manuscript to avoid confusion and to simplify the narrative. R-LP refers to the average value of lattice parameters, R-BL refers to the average value of T–O bond lengths, and R-MA refers to the mean of six O–T–O angles, in one tetrahedron from the references.

The chosen structures of albite and microcline from references had close degree of Al/Si order with their counterparts in this study.

The R-factors (Young, 1993) obtained from diffraction data of samples as well as respective refined cell parameters of albite and microcline are listed in Table 2, and R-LP of albite and microcline are reported in Table 2. The refined structure parameters of albite in the ALBITE sample, albite in the PERTHITE sample, and microcline in the PERTHITE sample are shown in Tables S1, S2, and S3, respectively. Figures 3 and 4 show the diffraction patterns and Rietveld fits of ALBITE and PERTHITE XRPD data, respectively. To prove the efficiency of SDCs, four T–O distances in each tetrahedron from the Albite–N model,

the Albite model, and the average from the references (R-BLA) are plotted in Figure 5, and their corresponding means of four T–O distances in each tetrahedron and the calculated value in terms of Equation (1) are shown in Figure 5. Similarly, for the PERTHITE sample, Figure S3 shows the four T–O distances in each tetrahedron from albite and from the average of the reference data (R-BLA), their corresponding means, and the calculated value in terms of Equation (1). Figure S4 shows the T–O distances in four tetrahedrons from microcline and from the average of the reference data (R-BLM), their corresponding means of four T–O bond lengths in each tetrahedron, and the calculated value in terms of Equation (2). Figure S5 shows the six O–T–O angles in each tetrahedron in albite from the model Albite–N, the model Albite, the albite in the PERTHITE sample, and the average from the references (R-MAA). These O–T–O angles in microcline from the PERTHITE sample and the average from the references (R-MAM) are shown in Figure S6.

Results showed that R factors decreased when SDCs were not applied (Model Albite–N and Model Albite were applied without and with SDCs in Table 2, respectively). SDCs had little effect on lattice parameters from Albite–N and Albite, and their differences of lattice parameters were about ±1 σ. The lattice parameters of albite in the ALBITE sample agreed with those of albite in the PERTHITE sample, and both approached R-LP of albite from those references. For albite, the differences of lattice parameters in this paper and R-LP were less than ±10 σ. The lattice parameters of microcline in the PERTHITE sample were close to R-LP, and their differences were about ±13 σ.

PM

Table 2. *R* factors, lattice paramters of albite in the ALBITE sample, and lattice parameters of albite and microcline in the PERTHITE sample; group space C$\bar{1}$.

R factors	R_{wp}	R_p	R_{exp}	χ^2	R_F^2	
Albite–N	13.6	8.75	10.6	1.67	6.25	
Albite	14.4	9.30	9.89	2.12	8.19	
PERTHITE	12.9	9.59	7.04	3.35	8.19	
Lattice parameters	*a*	*b*	*c*	α	β	γ
Albite–N[*]	8.1429(6)	12.7855(8)	7.1595(4)	94.245(3)	116.609(2)	87.679(4)
Albite[*]	8.1422(6)	12.7846(10)	7.1590(5)	94.243(3)	116.608(2)	87.681(4)
albite in PERTHITE[*]	8.1338(20)	12.8516(73)	7.1531(14)	94.368(34)	116.535(12)	87.729(46)
microcline in PERTHITE[*]	8.5888(13)	12.9656(21)	7.2234(11)	90.667(4)	115.983(3)	87.774(6)
Average lattice parameters from albite references (R-LPA)[**]	8.139(2)	12.784(2)	7.158(3)	94.24(2)	116.60(2)	87.72(2)
Average lattice parameters from microcline references(R-LPM)[**]	8.5692(4)	12.9646(7)	7.2190(3)	90.619(6)	115.911(5)	87.748(6)

Note: [*] Estimated standard deviation was obtained after the refinement was completed.

[**] Estimated standard deviation was averaged from the references.

The differences of most atomic coordinates appeared at three decimal places for these structural data of alkali feldspar in this paper and the references (Brown, 1961; Ribbe et al., 1962; Brown and Bailey, 1964; Ribbe et al., 1969; Dal Negro et al., 1978; Harlow and Brown Jr, 1980; Blasi et al., 1984; Blasi et al., 1987; Armbruster et al., 1990; Downs et al., 1994; Allan and Angel, 1997; Meneghinello et al., 1999). Although U_{iso} values of microcline and albite were obviously larger than published values (Ribbe et al., 1969; Blasi et al., 1984; Dal Negro et al., 1978; Downs et al., 1994), they were still reasonable. Furthermore, severe preferred orientations for the two samples in this study were observed by the authors and were verified by higher texture indexes (i.e., 6.74 for albite in the ALBITE sample; 3.30 for albite and 4.02 for microcline in the PERTHITE sample). This finding agreed with the report by Balic-Zunick et al. (2013).

DISCUSSION

Al/Si occupancies in albite and microcline were calculated from BB–XRPD via the lattice parameter method of Kroll and Ribbe (1987). The Al occupancies in albite structure from these two samples are equal to those based on the calculated Al contents (Tables S1 and S2). Thus, the Al atom completely occupies the T_1o tetrahedron, and the Si atom occupies other three tetrahedrons. The order degree in the two albite structure in this study reaches the maximum, and they are both low albite. The Al occupancies of microcline in the PERTHITE sample are 0.96, 0.02, 0.01, and 0.01 in T_1o,

T_1m, T_2o, and T_2m tetrahedrons, respectively. This finding shows that the microcline in the PERTHITE sample is highly ordered.

When SDCs were introduced in the structural model Albite, the individual and average T–O bond lengths in each tetrahedron closely approached the corresponding values of R-BL of albite (Figure 5). Whether SDCs were introduced in the structural model or not, the average <T–O> length was very close to the mean of R-BL (Figure 5), which agreed with the conclusions of Armbruster et al. (1990) and Angel et al. (2013), who both showed that the average <T–O> length was relatively insensitive to refinement strategies and models. Although the average T–O bond length in each tetrahedron approached that from R-BL, the individual T–O bond lengths obviously scattered and deviated from R-BL when SDCs were not introduced (Figure 5). Compared with the data from R-BL of albite, the differences for individual T–O bond length decreased from about ±0.036 Å (±36 σ) to ±0.004 Å (±4 σ) when SDCs were introduced. The relative contribution of SDCs to the total χ^2 in the final stage of the refinement was 13.0%, and then the introduction of SDCs in the structural model did play a key point during the refinement and efficiently improved the reliability of the structural data of albite. In fact, SDCs are often introduced as a routine tactic during Rietveld refinement. The accuracy and precision of the structural data both improved when SDCs were introduced in previous papers (Smrcok, 1995; Tribaudino et al., 2005; Tribaudino and Ohashi, 2011). Smrcok (1995) compared powder diffraction studies
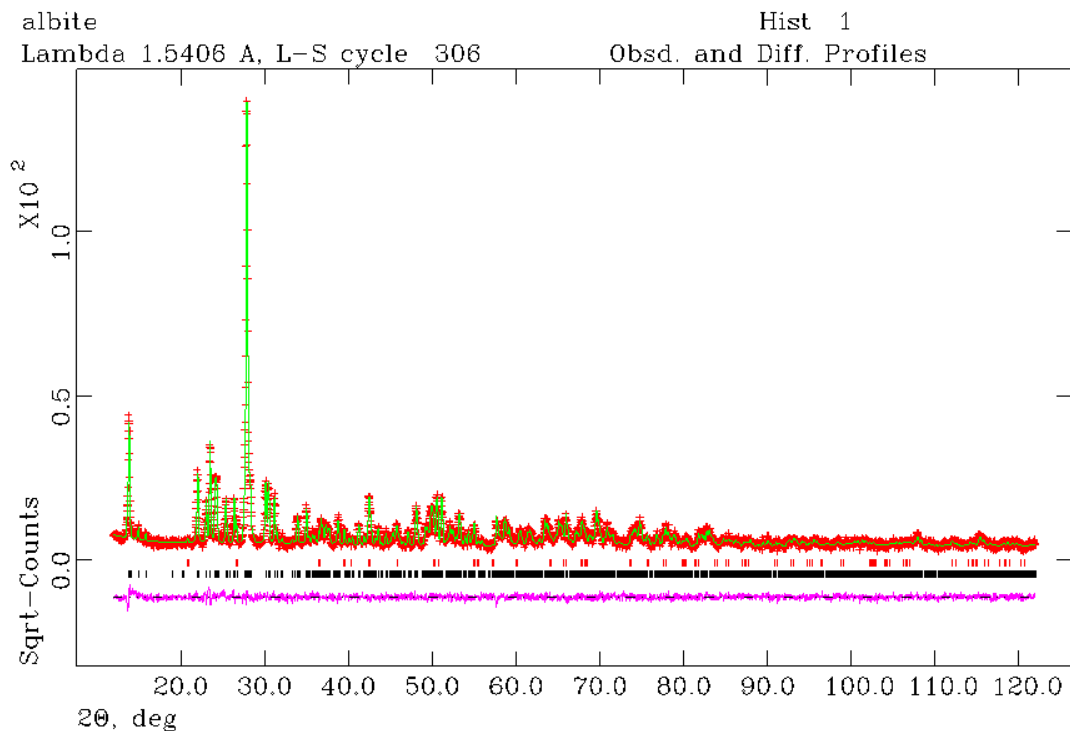
Figure 3. Rietveld plots of ALBITE sample. The upper curves are observed (crosses) and calculated (line) diffraction patterns. The lower curve shows the difference between observed and calculated patterns. Vertical marks at the bottom indicate the positions of allowed $K_{\alpha 1}$ and $K_{\alpha 2}$ reflections for albite and quartz from bottom to top, respectively.
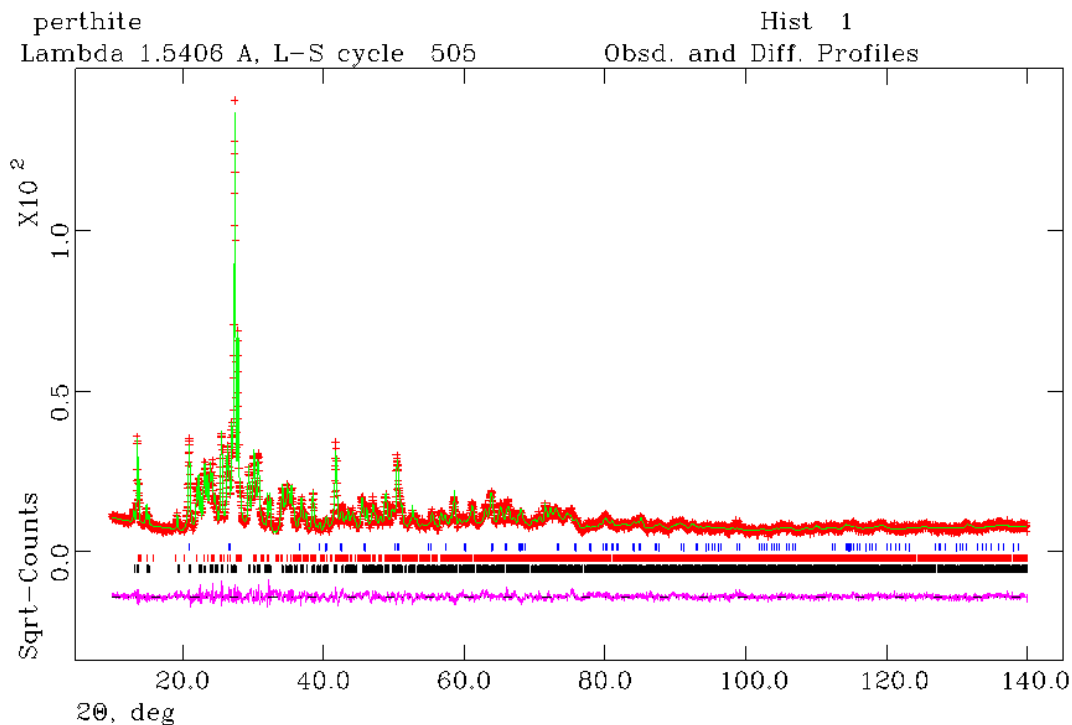
Figure 4. Rietveld plots of PERTHITE sample. The upper curves are observed (crosses) and calculated (line) diffraction patterns. The lower curve shows the difference between observed and calculated patterns. Vertical marks at the bottom indicate the positions of allowed $K_{\alpha 1}$ and $K_{\alpha 2}$ reflections for microcline, albite, and quartz from bottom to top, respectively.
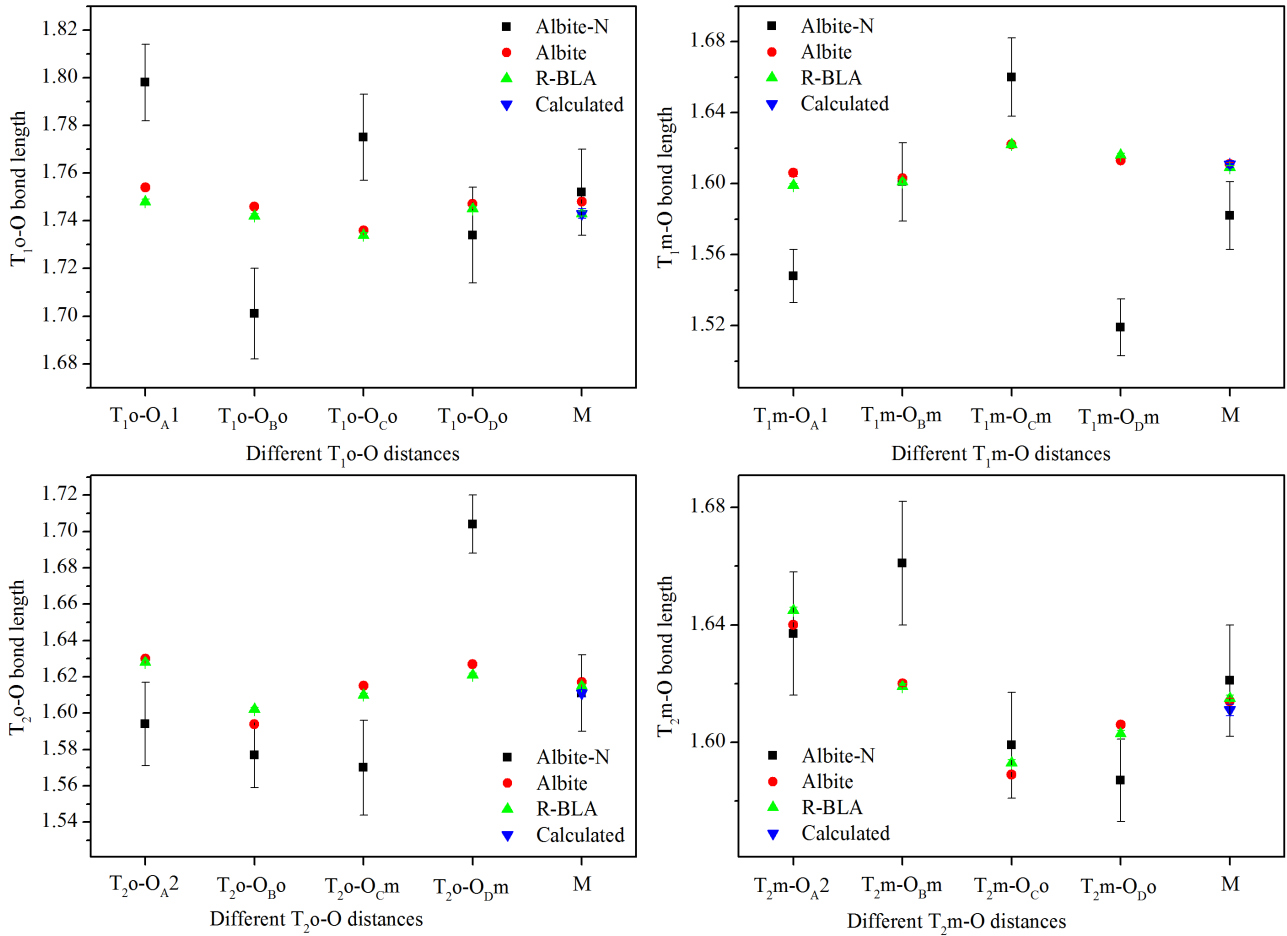
Figure 5. T–O distances in the tetrahedron of albite in the ALBITE sample from model Albite–N, model Albite, and those from albite references (R-BLA). M denotes the mean for Albite–N, Albite, R-BLA, and calculated value in terms of Equation (1); ■Albite–N; ●Albite; ▲R-BLA; ▼Calculated. The vertical bars represent errors. If no bar is given, then the error is contained within the area of the symbol.

of kaolinite and reported that refinements from neutron data (Suitch and Young, 1983; Young and Hewat, 1988) provide significantly poorer results than those from X-ray data (Bish and Von Dreele, 1989). This result was due to the refinement strategy because the formers did not introduce numerous soft constraints in their refinements, but the latter did. However, in this study, the introduction of SDCs was not a simple copy of the kaolinite example, and it was a combination between the two equations and soft distance constraints for Al/Si–O bond lengths, namely, a combination between the valence-bond theory and the Rietveld method. Therefore, the authors believe that this was an innovation of method to refine the feldspar structure by XRPD.

Basing on the successful case of extracting the structural data of albite in the ALBITE sample (it contains 99.3% albite and 0.7% quartz by quantitative phase analysis), the authors also succeeded in extracting albite and microcline structural data in the PERTHITE sample (it

contains 70.4% microcline, 28.0% albite and 1.6% quartz by quantitative phase analysis) from BB–XRPD via the updated model in Figure 2. Careful inspection showed that the difference of individual T–O bond lengths of albite between these of this study and those of references was ±0.005 Å (±5 σ). The difference of microcline between these of this study and those of references was ±0.006 Å (±6 σ). Similarly, the average T–O bond lengths in each tetrahedron for albite and microcline approached those from references. The difference of individual O–T–O angles in albite between Albite and Albite–N models was ±1 σ. Therefore, SDCs slightly affected on the O–T–O angle. Except for few large deviations of O–T–O angles in T_1m, T_2o, and T_2m tetrahedrons, these O–T–O angle values in the tetrahedrons of albite from Albite, Albite–N, and PERTHITE were very close to those from references (Figure S5). Similarly, these O–T–O angles in the tetrahedrons of microcline from the PERTHITE sample approached those from references (Figure S6).

The authors used two powder samples from two different Chinese localities and compared them with samples from different localities with close chemical compositions elsewhere in the world. Undoubtedly, averaging these structural data from different samples decreased the uncertainty introduced by different samples and made the comparison convincing. However, uncertainty may be introduced by the Al/Si order degree even if the authors picked up the samples with close Al/Si order degree to these in this study. In alkali feldspar, the degree of Al/Si order is closely related to the T–O bond length. Therefore, the deviation of the order degree will undoubtedly take a direct effect on the accuracy of the T–O bond length. The efficiency of the applied model in this study will be challenged because SDCs play a key role to extract the high-quality structural data from BB–XRPD. By analyzing quantities of data, Kroll and Ribbe (1987) estimated that the standard deviation σ of t_i was about ± 0.01. For a linear relationship, $y=kx+b$, the propagation of error can be calculated by the following formula: $\partial y=k\partial x+x\partial k+\partial b$. Then, $\partial T–O$ was equal to $\pm 0.002–0.004$ and $\pm 0.002–0.003$ in terms of Equations (1) and (2), respectively, and the average standard deviation σ was ± 0.003 and ± 0.002 for albite and microcline, respectively. Finally, $\partial T–O/T–O$ was about $\pm 0.17\%$ and $\pm 0.15\%$ for albite and microcline, respectively. Considering the relative contributions (13.0% for albite in the ALBITE sample; 7.25% for albite and 18.2% for microcline in the PERTHITE sample) of SDCs to the total χ^2 in the final stages of refinement, the propagation of error, introduced through Equations (1) and (2), was 2.16% for albite in the ALBITE sample and 1.21% for albite and 2.71% for microcline in the PERTHITE sample. The propagation error introduced through Equations (1) and (2) was very small, and the uncertainty introduced via SDCs and the Al occupancy took a slight effect on the quality of the structural data in this paper. Angel et al. (2013) found that the influence of temperature, composition, or state of Al/Si order on the grand mean <<T–O>> bond lengths was statistically insignificant in the total population of structures, and the existing information in this study completely agreed with those found by Angel et al. (2013). The reference data, the calculated values from Equations (1) and (2), and the M values in Figures 5, S3, and S4 were close to each other. Therefore, the authors inferred that errors caused by a slight difference in order state and different composition did not significantly affect the comparison of structure data from this study and from the references. By comparing structural data from powder diffraction with those from other methods, Kaduk (1996) concluded that bond distances can be determined to an accuracy of 0.02 Å and bond angles can be accurately expected at 3°. In this paper, the values of T–O interatomic distances in Figures 5, S3, and S4 (most of less than ±0.01 Å) and the

values of O–T–O interatomic angles in Figures S5 and S6 (most less than ±1°) agreed with Kaduk's conclusion, and the quality of alkali feldspar structural data from BB–XRPD could be afforded to a certain degree.

By using appropriate refinement strategies, Liu et al. (2014a, 2014b) proved the feasibility of extracting high-quality structural data from XRPD by comparing XRPD data with those from X-ray single-crystal analysis for calcite and dolomite. However, the structural symmetry of albite and microcline is triclinic and is lower than those of calcite and dolomite. This causes severe overlapping of diffraction peaks for two samples in this study. Microstrain also existed in PERTHITE, but the preferred orientation and microstrain were both appropriately described in the structural model. The structures of albite and microcline closely approached those of the references (Brown, 1961; Ribbe et al., 1962; Brown and Bailey, 1964; Ribbe et al., 1969; Dal Negro et al., 1978; Harlow and Brown Jr., 1980; Blasi et al., 1984; Blasi et al., 1987; Armbruster et al., 1990; Downs et al., 1994; Allan and Angel, 1997; Meneghinello et al., 1999;) using the model in Figure 2. Therefore, the model in Figure 2 was successful, and this was further proved by good Rietveld fits of two samples (Figures 3 and 4).

CONCLUSIONS

In the final analysis, apart from appropriate strategies used during refinement, the high reliability of structural data for albite and microcline from BB–XRPD was mainly due to the calculation of two linear equations related to T–O bond length and Al/Si occupancy, application of SDCs, and tactical combination of two linear equations and SDCs. The model can be extended to other similar structures, such as natural minerals albite and microcline with different Al/Si order degree, as well as other natural or artificial minerals with the feldspar structure, for example, Li-feldspar [$LiAlSi_3O_8$], gallium albite [$NaGaSi_3O_8$], germanium albite [$NaAlGe_3O_8$], boron albite [$NaBSi_3O_8$] and buddingtonite [$N(D/H)_4AlSi_3O_8$], to extract high-quality structural data from XRPD. Therefore, BB–XRPD combined with Rietveld method potentially continues to have an important function in uncovering more structural details of minerals, in the future.

REFERENCES
Allan D. and Angel R., 2000. A high-pressure structural study of microcline ($KAlSi_3O_8$) to 7 GPa. European Journal of Mineralogy 9, 263-275.

Angel R., Ross N., Zhao J., Sochalski-Kolbus L., Kruger H., Schmidt B., 2013. Structural controls on the anisotropy of tetrahedral frameworks: the example of monoclinic feldspars. European Journal of Mineralogy 25, 597-614.

Armbruster T., Burgi H., Kunz M., Gnos E., Bronnimann S., Lienert C., 1990. Variation of displacement parameters in structure refinements of low albite. American Mineralogist 75, 135-140.

Bailey S. and Taylor W., 1955. The structure of a triclinic potassium feldspar. Acta Crystallographica 8, 621-632.

Balic-Zunic T., Piazolo S., Katerinopoulou A., Schmith J., 2013. Full analysis of feldspar texture and crystal structure by combining X-ray and electron techniques. American Mineralogist 98, 41-52.

Bish D. and Von Dreele R., 1989. Rietveld refinement of non-hydrogen atomic positions in kaolinite. Clays and Clay Minerals 37, 289-296.

Blasi A., Brajkovic A., De Pol Blasi C., Foord E., Martin R., Zanazzi P., 1984. Structure refinement and genetic aspects of a microcline overgrowth on amazonite from Pikes Peak batholith, Colorado, USA. Bulletin de Minéralogie 107, 411-422.

Blasi A., De Pol Blasi C., Zanazzi P., 1981. Structural study of a complex microperthite from anatexites at Mt. Caval, Argentera Massif, Maritime Alps. Neues Jahrbuch für Mineralogie - Abhandlungen 142, 71-90.

Blasi A., De Pol Blasi C., Zanazzi P., 1987. A reexamination of the Pellotsalo microcline: mineralogical implications and genetic considerations. The Canadian Mineralogist 25, 527-537.

Brown B., 1961. The crystal structure of maximum microcline. Thesis, University of Wisconsin-Madison.

Brown B. and Bailey S., 1964. The structure of maximum microcline. Acta Crystallographica 17, 1391-1400.

Dal Negro A., De Pieri R., Quareni S., 1978. The crystal structures of nine K feldspars from the Adamello Massif (Northern Italy). Acta Crystallographica B34, 2699-2707.

D'Amour H., Denner W., Schulz H., 1979. Structure determination of α-quartz up to 68×10^8 Pa. Acta Crystallographica B35, 550-555.

Downs R., Hazen R., Finger L., 1994. The high-pressure crystal chemistry of low albite and the origin of the pressured ependency of Al-Si ordering. American Mineralogist 79, 1042-1052.

Ferguson R., Traill R., Taylor W., 1958. The crystal structures of low-temperature and high-temperature albites. Acta Crystallographica 11, 331-348.

Finger L., Cox D., Jephcoat A., 1994. A correction for powder diffraction peak asymmetry due to axial divergence. Journal of Applied Crystallography 27, 892-900.

Finney J. and Bailey S., 1964. Crystal structure of an authigenic maximum microcline. Zeitschrift für Kristallographie 119, 413-436.

Harlow G. and Brown Jr. G., 1980. Low albite an X-ray and neutron diffraction study. American Mineralogist 65, 986-995.

Kaduk J., 1996. Chemical accuracy and precision in structural refinements powder diffraction data. Advances in X-ray analysis 40, 352-370.

Keefer K. and Brown G., 1978. Crystal structures and compositions of sanidine and high albite in cryptoperthitic intergrowth. American Mineralogist 63, 1264-1273.

Kroll H. and Ribbe P., 1987. Determining (Al, Si) distribution and strain in alkali feldspars using lattice parameters and diffraction-peak positions, A review. American Mineralogist 72, 491-506.

Larson A. and Von Dreele R., 2004. General Structure Analysis System (GSAS). Los Alamos National Laboratory Report (LAUR 86-748), Los Alamos, New Mexico, 224 pp.

Liu S., 2015. Rietveld structure refinement of microcline. European Journal of Mineralogy 27, 501-510.

Liu S., Li H., Liu J., 2014a. Reliability of the structural data for calcite and dolomite extracted from X-ray powder diffraction by Rietveld refinement. Periodico di Mineralogia 83, 121-140.

Liu S., Li H., Liu J., 2014b. Obtaining optimal structural data from X-ray powder diffraction using the Rietveld method. Powder Diffraction 29, 396-403.

Meneghinello E., Alberti A., Cruciani G., 1999. Order-disorder process in the tetrahedral sites of albite. American Mineralogist 84, 1144-1151.

Phillips M., Colville A., Ribbe P., 1971. The crystal structures of two oligoclases: A comparison with low and high albite. Zeitschrift für Kristallographie 133, 43-65.

Phillips M., Ribbe P., Pinkerton A., 1989. Structure of Intermediate Albite, $NaAISi_3O_8$. Acta Crystallographica C45, 542-545.

Prewitt C., Sueno S., Papike J., 1976. The crystal structures of high albite and monalbite at high temperatures. American Mineralogist 61, 1213-1225.

Ribbe P., 1979. The structure of a strained intermediate microcline in cryptoperthitic association with twinned plagioclase. American Mineralogist 64, 402-408.

Ribbe P., 1983. Aluminum-silicon order in feldspars, domain textures and diffraction patterns. In: Ribbe P. (ed) Feldspar Mineralogy, 2. Reviews in Mineralogy, Mineralogical Society of America, Chantilly, Virginia, pp. 21-56.

Ribbe P., Ferguson R., Taylor W., 1962. A three-dimensional refinement of the structure of low albite. Norsk Geologisk Tidsskrift 42, 152-157.

Ribbe P., Megaw H., Taylor W., Ferguson R., Traill R., 1969. The albite structures. American Mineralogist B25, 1503-1518.

Rietveld H., 1967. Line profiles of neutron powder-diffraction peaks for structure refinement. American Mineralogist 22, 151-152.

Rietveld H., 1969. A profile refinement method for nuclear and magnetic structures. Journal of Applied Crystallography 2, 65-71.

Smrcok L., 1995. A comparison of powder diffraction studies of kaolin group minerals. Zeitschrift für Kristallographie 210, 177-183.

Suitch P. and Young R., 1983. Atom positions in highly ordered kaolinite. Clays and Clay Minerals 31, 357-366.

Toby B., 2001. EXPGUI, a graphical user interface for GSAS. Journal of Applied Crystallography 34, 210-213.

Tribaudino M., Angel R., Cámara F., Nestola F., Pasqual D., Margiolaki I., 2010. Thermal expansion of plagioclase feldspars. Contributions to Mineralogy and Petrology 160, 899-908.

Tribaudino M., Bruno M., Nestola F., Pasqual D., Angel R.,

2011. Thermoelastic and thermodynamic properties of plagioclase feldspars from thermal expansion measurements. American Mineralogist 96, 992-1002.

Tribaudino M., Nestola F., Meneghini C., 2005. The structure behaviour of intermediate pyroxenes along the diopside-enstatite join. The Canadian Mineralogist 43, 1411-1421.

Tribaudino M. and Ohashi H., 2011. High temperature structure and thermal expansion of $Co_3Al_2Si_3O_{12}$ garnet. Periodico di Mineralogia 80, 135-144.

Wang Z., Chen G., Shao W., 1982. Genetic mineralogy of albites in lujia gold deposit. Journal of Graduate School, China University of Geosciences 12, 210-213.

Wenk H. and Kroll H., 1984. Analysis of P-1, I-1, and C-1 plagioclase structures. Bulletin de Mineralogie 107, 467-487.

Winter J., Okamura F., Ghose S., 1979. A high temperature structural study of high albite, monalbite and the analbite-monalbite phase transition. American Mineralogist 64, 409-423.

Young R., 1993. The Rietveld Method. Oxford University Press, New York.

Young R. and Hewat A., 1988. Verification of the triclinic crystal structure of kaolinite. Clays and Clay Minerals 36, 225-232.

Zucchini A., Comodi P., Katerinopoulou A., Balic-Zunic T., McCammon C., Frondini F., 2012. Order-disorder-reorder process in thermally treated dolomite samples: a combined powder and single-crystal X-ray diffraction study. Physics and Chemistry of Minerals 39, 319-328.